VNU Journal of Science: Natural Sciences and Technology, Vol. 39, No. 3 (2023) 90-99

VNU Journal of Science: Natural Sciences and Technology

Journal homepage: https://js.vnu.edu.vn/NST

Original Article

A Novel Heterojunction $CuWO_4$/g-C_3N_4 Photocatalyst for Removal of Methylene Blue from Aqueous Solution under Visible Light Irradiation

Do Van Dang[1,*], Le Thanh Son[1], Nguyen Huy Hai[2]

[1]*VNU University of Science, 334 Nguyen Trai, Thanh Xuan, Hanoi, Vietnam*
[2]*VNU HUS High School for Gifted Students, 182 Luong The Vinh, Thanh Xuan, Hanoi, Vietnam*

Received 14 May 2023
Revised 25 May 2023; Accepted 25 May 2023

Abstract: In this study, a series of $CuWO_4$/g-C_3N_4 composites were synthesized using a facile construction method. The structural characteristics of the composites were examined using various techniques, including XRD, SEM, SEM-EDS, FT-IR, and UV-DRS. The photocatalytic performance of the $CuWO_4$/g-C_3N_4 nanocomposites was evaluated in the degradation of methylene blue (MB) under visible light irradiation. The findings revealed that the $CuWO_4$/g-C_3N_4 composite with a mass ratio of 10% $CuWO_4$ displayed the highest efficiency (89%) in degrading MB during an 80-minute photodegradation process, which was consistent with the pseudo-first-order kinetics. These results demonstrate that forming a Z-scheme $CuWO_4$/g-C_3N_4 heterojunction significantly improves the photocatalytic efficiency by promoting rapid separation of electron-hole pairs and enhancing the redox capability. Additionally, the photodegradation efficiency remained above 85% even after four cycles, suggesting the stability of the catalyst.

Keywords: Z- scheme, $CuWO_4$/g-C_3N_4, Methylene blue, photodegradation, visible light.

1. Introduction

Due to the rapid growth of industrial activities, various types of pollutants, including pharmaceutical products, dyes, and pesticides, have been released into water bodies, causing severe ecological damage [1]. Methylene Blue (MB), a commonly used dye, has been found to have potentially harmful effects on human health, such as non-lethal mutagenicity and adverse impacts on lung function. Fortunately, there are several conventional techniques available for removing MB from water solutions, including bio-sorption [2], electrochemical treatment [3], adsorption [4], and photocatalysis [5]. Advanced oxidation processes (AOPs) are considered an innovative approach to degrade MB because of their strong ability to break it down completely [6]. Recently, semiconductor photocatalysts, particularly those driven by visible light, have gained significant attention as a promising

* Corresponding author.
E-mail address: dangdovan@hus.edu.vn

https://doi.org/10.25073/2588-1140/vnunst.5559

technology for water purification. Visible light-driven semiconductors are particularly valuable due to their ability to utilize sunlight from the solar spectrum, facilitated by their low energy band gaps. Among them, g-C_3N_4, a polymeric semiconductor, has attracted increasing interest since the discovery of its ability to produce hydrogen through photocatalysis in 2009 [7-9]. Although g-C_3N_4 has a moderate energy band gap (~ 2.7 eV) that allows it to absorb visible light effectively, its valence band potential (VBP) exhibits limited oxidation ability, leading to the fast recombination of electrons and holes, which hinders its practical applications. Therefore, there is a strong motivation to develop suitable modifications to enhance the photocatalytic efficiency of g-C_3N_4 [7-9].

Several approaches have been employed to address these difficulties by modifying the surface area, electronic energy level, and energy band gap of g-C_3N_4. One effective strategy to enhance its photocatalytic efficiency is forming a heterojunction system by combining g-C_3N_4 with other materials. The structure of g-C_3N_4, which consists of 2D layers, facilitates easy modification and heterojunction formation. The conventional heterojunction (referred to as a type II heterojunction) created by combining g-C_3N_4 with a suitable semiconductor effectively prevents the recombination of electrons and holes [10, 11]. However, their redox potentials are insufficient for the complete degradation of organic compounds, thereby limiting their photocatalytic efficiency.

To overcome the limitations of conventional heterojunctions, the construction of a Z-scheme heterojunction has been recognized as a promising approach. In Z-scheme photocatalysts, electrons generated by component A with a lower reduction potential can transfer to the valence band of component B, resulting in strong reduction-oxidation potentials and simultaneous charge separation. The conduction band potential (CBP) of g-C_3N_4 is approximately -1.4 eV, which makes it highly suitable for photocatalytic reduction reactions. Hence, it can be combined with various n-type photocatalysts to establish a Z-scheme heterojunction [10, 11]. Recently, there has been a surge of interest in tungstate metal (MWO_4) materials due to their distinctive chemical and optical properties. Among them, $CuWO_4$ has gained popularity in photocatalysis due to its narrow band gap (2.3 eV) and its ability to be easily excited by visible light. The valence band (VB) and conduction band (CB) potentials of $CuWO_4$ are approximately 2.83 and 0.63 V, respectively, making it compatible with g-C_3N_4 to form a Z-scheme heterojunction. This heterojunction enhances their light absorption capacity and extends the lifetime of the charges they produce [12-18].

In 2021, Zhou and colleagues reported on the development of $CuWO_4$/g-C_3N_4 for Rhodamine B (RhB) degradation under visible light exposure [15]. After 150 minutes of visible light irradiation, up to 93% of RhB was removed, and the synthesized material exhibited stability, allowing it to be reused for at least four cycles without a decline in photocatalytic activity. The following year, the Vinesh group reported on the application of $CuWO_4$/g-C_3N_4 nanocomposite for the removal of tetracycline hydrochloride (TCH) [12]. The $CuWO_4$/g-C_3N_4 nanocomposite demonstrated a significantly enhanced photocatalytic degradation of tetracycline (TC) compared to pristine g-C_3N_4, with an improvement of approximately 7.4 times in 120 minutes. The enhanced photocatalytic activity of the heterojunction materials can be attributed to the unobstructed separation and transfer of photogenerated carriers, facilitated by the well-matched energy band structure between $CuWO_4$ and g-C_3N_4, thereby promoting the photodegradation of organic pollutants.

Taking these factors into account, we focused our efforts on constructing a $CuWO_4$/ g-C_3N_4 Z-scheme heterojunction for the

efficient photocatalytic degradation of MB under visible light irradiation.

2. Experimental Section

2.1. Chemicals

Melamine ($C_3H_6N_6$), Copper Nitrate Hexanhydrate ($Cu(NO_3)_2.6H_2O$), Sodium Tungstate Dehydrate ($Na_2WO_4.2H_2O$), Methylene Blue ($C_{16}H_{18}ClN_3S$), Sodium hydroxide (NaOH) and Hydrochloric acid (HCl) were purchased from Sigma Aldrich. All compounds were used directly without further purification.

2.2. Catalyst Preparation

$CuWO_4$ nanoparticles were prepared in accordance with a previous report [12]. Firstly, 4 mmol of $Cu(NO_3)_2.6H_2O$ was added to 50 mL of distilled water, followed by the dropwise addition of a 0.08 M Na_2WO_4 solution. The suspension was stirred for 4 hours, and the resulting precipitate was separated via centrifugation and dried at 60 °C for 24 hours before being transferred to a furnace. The furnace was heated continuously to 500 °C with a rate of 5 °C per minute and kept at that temperature for 2 hours to obtain $CuWO_4$.

The g-C_3N_4 was prepared following the previous report published anywhere [19]. Melamine was calcinated at 550 °C for 4 h to prepare g-C_3N_4 as a yellow powder.

In order to construct of heterostructure $CuWO_4$/g-C_3N_4 nanocomposite, a mixture of $CuWO_4$ and g-C_3N_4 was sonicated in 100 mL of distilled water for 1 hour, with varying mass ratios of $CuWO_4$/g-C_3N_4) = 1/50, 1/20, 1/10 and 1/5. The resulting suspension was heated in an autoclave at 160 °C for 12 hours. The solid was filtrated and washed with water to get the x$CuWO_4$/g-C_3N_4 nanocomposite (x = 2%, 5%, 10%, and 20%, respectively).

2.3. Characterization

Standard powder X-ray diffraction (XRD) patterns were performed on a D8-Advance-Brucker. A Bruker TENSOR-27 was used to achieve Fourier transform infrared spectroscopy (FTIR) spectra. The Hitachi S-4800 microscope was used to obtain scanning electron micrograph (SEM) images of synthesized materials. Scanning Electron Microscopy with Energy Dispersive Spectroscopy (SEM-EDS) images were measured on an Oxford instrument with detector X-stream 2 (EDX pulse processor). Ultraviolet-visible light absorption spectra (UV-Vis) were obtained using a Hitachi UH4150 spectrophotometer to analyze optical properties.

2.4. Photodegradation of MB

In a typical experiment, 100 mg of catalysts were mixed with 100 mL of 10 mg. L^{-1} MB solution was stirred in the dark for 30 minutes until adsorption-desorption equilibrium was reached. Subsequently, the mixture was exposed to a 200 W LED in a photoreactor located 5 cm away from the deflection reflector. Samples of 2 mL were taken every 20 minutes during irradiation and analyzed for MB degradation using a UV-VIS spectrophotometer (F7G32AA/Agilent) at 665 nm. The pH of the solutions was adjusted to between 3 and 9 using 1 M NaOH and HCl solutions and monitored with a Mettler Toledo pH meter.

Direct photolysis of MB without a catalyst (using only light) was also examined under identical conditions to provide a basis for comparison. The percentage (%) of MB removal was calculated using Equation (1), while Equation (2) was utilized to determine the kinetics of MB dye removal via the photocatalytic process for the first order with the corresponding time. Where C_0 denotes the initial concentration of MB solution in adsorption-desorption equilibrium (mg. L^{-1}), C_t represents the final concentration of the dye solution after treatment (mg. L^{-1}), and k (min^{-1}) represents the reaction kinetic rate constant for a first-order process.

$$\% \text{ Removal} = \frac{C_o - C_t}{C_o} \times 100 \quad (1) \qquad \ln\frac{C_o}{C_t} = kt \quad (2)$$

To evaluate the photocatalyst's reusability, the photocatalyst was collected after the reaction through centrifugation, washed with

ethanol and distilled water, and dried under vacuum at 60 °C for 6 hours before being employed for the next cycle.

3. Results and Discussion

3.1. Characterization of Materials

Figure 1 displays the XRD patterns of pure $CuWO_4$, g-C_3N_4, and $CuWO_4$/g-C_3N_4 composite with varying amounts of $CuWO_4$.

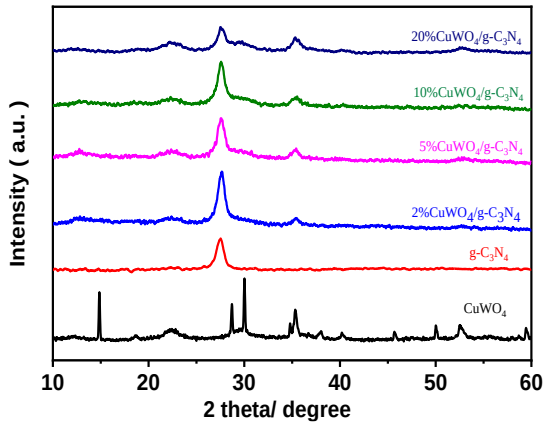

Figure 1. XRD patterns of synthesized materials.

The XRD pattern of pure $CuWO_4$ shows the diffraction peaks at 2θ of 15,43º, 18,84º, 22,5º, 28,75º, 30,60º, 35,81º, 39,82º, and 53.3°, which can be indexed as the (110), (100), (011), (111), (111), (002), (120), and (221), respectively. The result indicated that the patterns disclosed the standard for typical monoclinic crystal wolframite planes of $CuWO_4$ according to JCPDS no. 01-070-1732 [12]. In addition, the absence of information on other Copper or tungstate products from the XRD pattern further confirmed the successful preparation of $CuWO_4$. The g-C_3N_4 material exhibited two peaks with 2θ values of 13.1° and 27.8° in its X-ray diffraction (XRD) pattern. The peak at 27.8° corresponded to the (002) crystal plane of the conjugated aromatic system, while the peak at 13.1° was related to the distance between the nitride pores (JCPDS: 50-1512) [19]. It is important to note that the XRD patterns of $CuWO_4$ and g-C_3N_4 were still discernible in the $CuWO_4$/g-C_3N_4 composite without the decrease in intensity. These findings suggest that the composite maintained its structured regularity during construction, which is consistent with earlier studies.

Figure 4 displays the FT-IR spectra of the prepared g-C3N4, CuWO4, and CuWO4/g-C3N4 nanocomposite to further confirm the composite's success. The g-C_3N_4 FT-IR spectrum showed 810 and 3200 cm-1 peaks, corresponding to the breathing modes of the tris-triazine units and residual N–H groups, respectively. Additionally, peaks between 1200 cm^{-1} and 1700 cm^{-1} were caused by the stretching vibration modes of the C-N group and the stretching of the C=N group [19]. In Figure 3b, the strong, broad band observed in the 400- 1000 cm^{-1} low-frequency region was attributed to the characteristic deformation modes of Cu-O, W-O, and W-O-W bridges. The $CuWO_4$/g-C_3N_4 FT-IR spectrum exhibited similar peaks to those of g-C_3N_4 but with lower peak intensities due to the deposition of $CuWO_4$ on the g-C_3N_4.

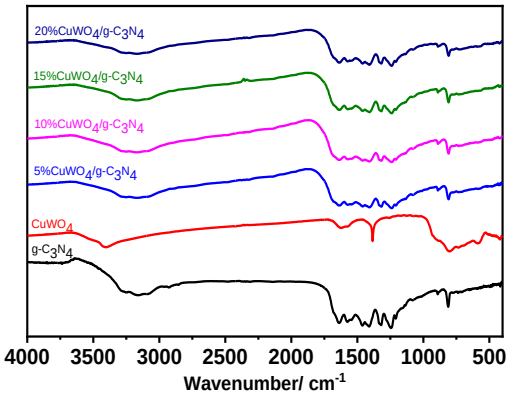

Figure 2. FT-IR of synthesized materials.

The pure CuWO4, g-C3N4, and CuWO4/g-C3N4 composite morphologies were analyzed using SEM images (Figure 3). The SEM images showed the excellent distribution of nanolayer structures of g-C_3N_4 resulting from polymerization (Figure 2a). It can be observed that the synthesized $CuWO_4$ sample consisted of nanospheres that were randomly assembled with each other. However, it was hard to observe the $CuWO_4$ nanoparticle in the

$CuWO_4/g\text{-}C_3N_4$ composite due to the presence of $g\text{-}C_3N_4$ presented in the cluster of $CuWO_4$. To further confirm the successful construction of the $CuWO_4/g\text{-}C_3N_4$ composite, the SEM-EDS analysis of the $10\%CuWO_4/g\text{-}C_3N_4$ composite's elemental composition and distribution is shown in Figures 3d and 4. The findings revealed that $CuWO_4$ was uniformly dispersed in $g\text{-}C_3N_4$, with no other atoms detected, indicating successful composite synthesis. Furthermore, the SEM-EDX results allowed fitting the element's components to the composite's formula.

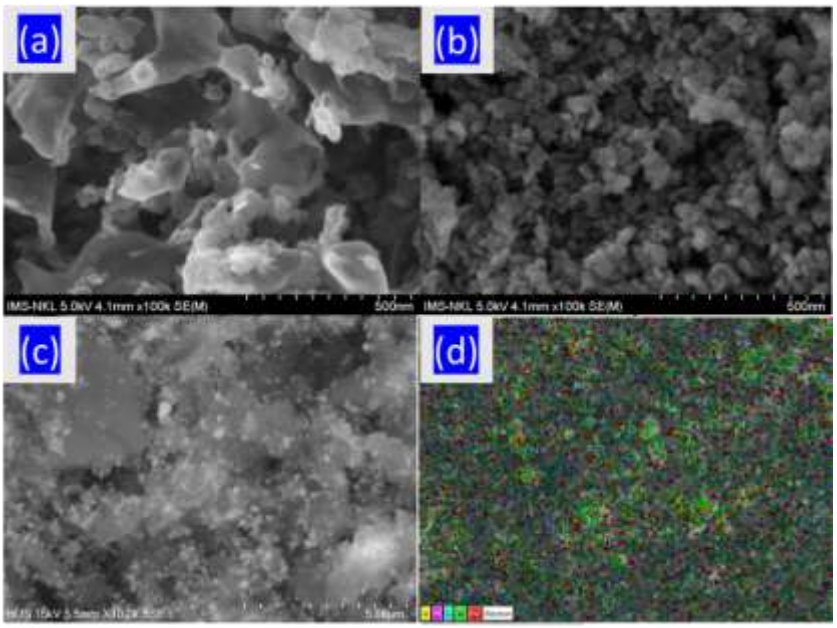

Figure 3. SEM images of (a) $g\text{-}C_3N_4$; (b) $CuWO_4$; (c) $10\%CuWO_4/g\text{-}C_3N_4$; (d) SEM-EDS of $10\%CuWO_4/g\text{-}C_3N_4$.

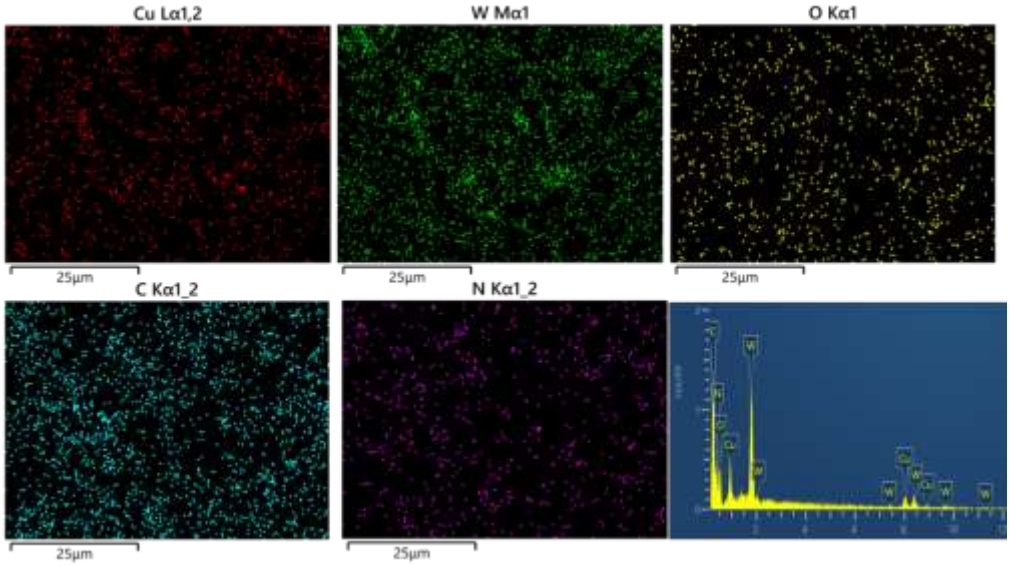

Figure 4. Element mapping and SEM-EDX of 10%CuWO4/g-C3N4.

Optical characteristics are generally understood to be critical in determining a catalyst's photo activity. To investigate the effect of $CuWO_4$ nanoparticles incorporation on g-C_3N_4, the UV-DRS spectra of pure g-C_3N_4, $CuWO_4$, and $CuWO_4$/g-C_3N_4 composite with varying $CuWO_4$ content were analyzed and shown in figure 5. Pure g-C_3N_4 displays a prominent absorption peak around 400 nm corresponding to the $\pi \rightarrow \pi^*$ and $n \rightarrow \pi^*$ transitions happening within the tri-s-zine or tri-s-heptazine units. On the other hand, the absorption spectra of $CuWO_4$ reveal a broad absorption range spanning from 300 to 525 nm. This absorption can be attributed to the transition of electrons from the valence band, occupied by hybridized O-2p and Cu-3d orbitals, to the conduction band composed of W-5d orbitals. Notably, the presence of $CuWO_4$ on the surface of g-C_3N_4 led to a shift towards longer wavelengths, resulting in increased absorption within the visible light range when compared to g-C_3N_4.

The bandgap of all materials was determined through Tauc plots based on matching DRS absorption spectra. The Tauc plots of g-C_3N_4 and x$CuWO_4$/g-C_3N_4 are presented in Figure 5. The bandgap of x$CuWO_4$/g-C_3N_4 (with 2, 5, 10, and 20 wt% of $CuWO_4$) produced values of 2.19 eV, 2.1 eV, 1.99 eV, and 2.0 eV, respectively, which were considerably lower than that of pure g-C_3N_4 (2.71 eV). These findings indicate that $CuWO_4$/g-C_3N_4 materials are more active than g-C_3N_4 when exposed to visible light.

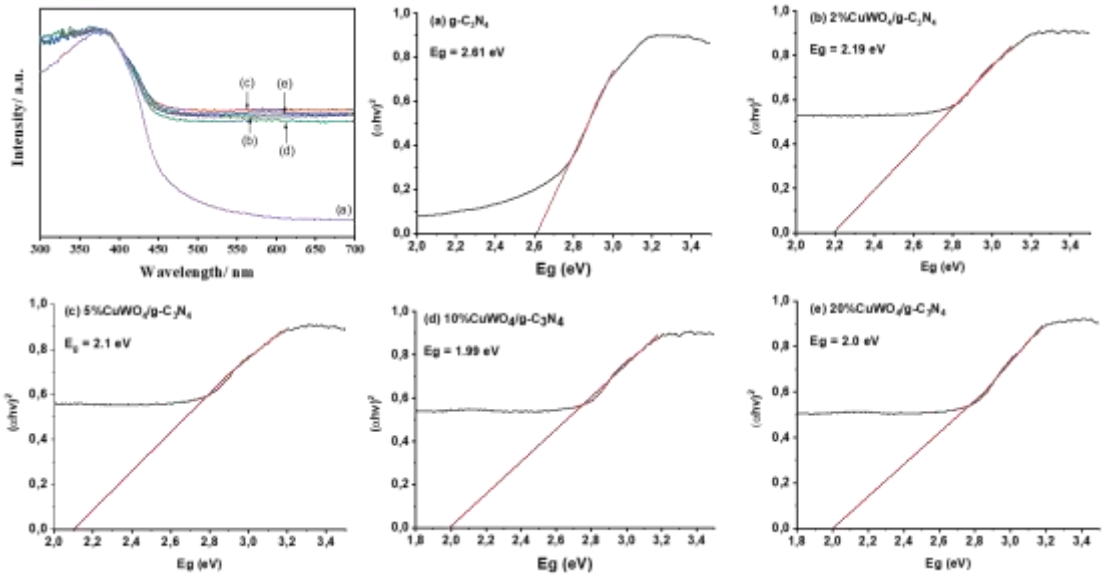

Figure 5. UV DRS and Tauc plot of (a) g-C_3N_4; (b) 2%$CuWO_4$/g-C_3N_4; (c) 5%$CuWO_4$/g-C_3N_4; (d) 10%$CuWo_4$/g-C_3N_4; (e) 20%$CuWO_4$/g-C_3N_4.

3.2. Photodegradation of MB

The ability of the $CuWO_4$/g-C_3N_4 composite to undergo photocatalysis was investigated in the photodegradation of MB in water under visible light irradiation. In the absence of light, no MB degradation occurred, as indicated by the negligible decrease in MB concentration, which can be attributed to adsorption on the material's surface (data not presented here). However, after 80 minutes of visible light irradiation, a moderate yield of MB degradation (40%) was observed in the presence of the $CuWO_4$ photocatalyst compared to g-C_3N_4 (60%). This outcome can be attributed to the rapid recombination of photogenerated electron and hole pairs, despite

the $CuWO_4$'s low bandgap of 2.2 eV. Moreover, the photodegradation of MB declined in the absence of a catalyst, suggesting that $CuWO_4$/g-C_3N_4 and visible light irradiation were necessary for the photodegradation of MB.

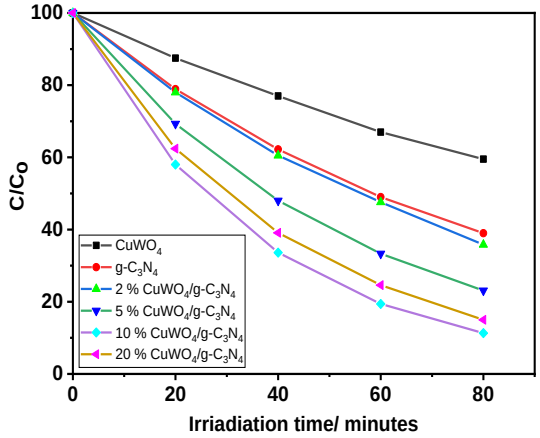

Figure 6. Photodegradation of MB using synthesized catalyst under visible light irradiation.

Furthermore, as the loading amount of $CuWO_4$ on g-C_3N_4 increased from 2% to 10%, the removal efficiency of MB exhibited a substantial enhancement of approximately 64%, 77%, and 89%, respectively. This improvement can be attributed to the reduction in the band gap from 2.19 eV to 1.99 eV, making the composite more active under visible light irradiation. The findings were further supported by the hindrance of electron-hole recombination, leading to an augmented photocatalytic activity, as indicated by the UV-DRS spectra. Interestingly, when 20% $CuWO_4$/g-C_3N_4 was employed as the catalyst, the degradation yield of MB was only 85%, resulting in a slight decrease despite its lower band gap of 2.0 eV. The substantial amount of CuWO4 can explain this added, which hinders the light absorption of g-C_3N_4 responsible for dye degradation, thereby confirming a decline in photocatalytic activity. Moreover, the photodegradation of MB under visible light irradiation was remarkably insignificant in the absence of a catalyst. Based on these results, the 10%$CuWO_4$/g-C_3N_4 composite was selected as the photocatalyst for subsequent experiments.

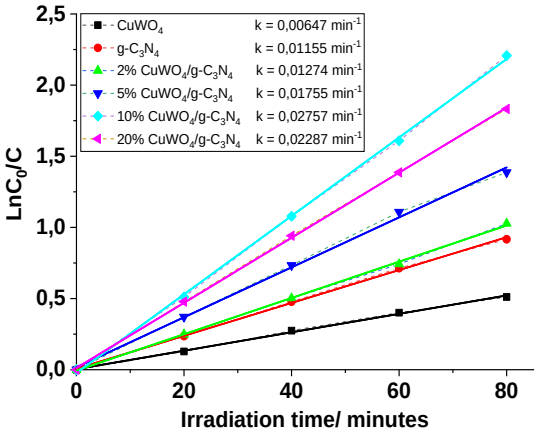

Figure 7. Pseudo-first-order model of MB photodegradation using 10%$CuWO_4$/g-C_3N_4.

In order to examine the reaction kinetics of MB degradation using $CuWO_4$/g-C_3N_4, the degradation data was analyzed using a pseudo-first-order model (Equation 2). Figure 7 presents the correlation between $\ln(C_0/C_t)$ and the exposure time for MB degradation on the catalysts. The photodegradation curve closely followed the pseudo-first-order kinetics for all tested scenarios. The rate constants (k) for each catalyst were determined and plotted in Figure 7 using the model. As the $CuWO_4$ loading on the surface of g-C_3N_4 increased, the rate constants exhibited a notable increase as well. Notably, the 10% $CuWO_4$/g-C_3N_4 catalyst displayed the highest rate constant (0.02757 min^{-1}) for MB degradation among the photocatalysts. This value considerably exceeded those reported in recent studies for other photocatalysts.

A series of experiments were conducted to assess the influence of different quantities of the 10%CuWO4/g-C3N4 catalyst on MB elimination. The catalyst amounts ranged from 0.5 to 1.5 $g.L^{-1}$ while maintaining a consistent MB concentration of 10 $mg.L^{-1}$ and pH 7.0. The experimental outcomes were presented in Figure 8, revealing a significant enhancement in MB removal with increasing catalyst amount from 0.5 to 1.0 $g.L^{-1}$. However, further increases in catalyst concentration did not lead to improved photodegradation of MB. This lack of improvement could be attributed to the excessive suspension of the catalyst, hindering

light penetration to the MB molecules. Consequently, the researchers proceeded with a catalyst amount of 1.0 $g.L^{-1}$ for subsequent experiments.

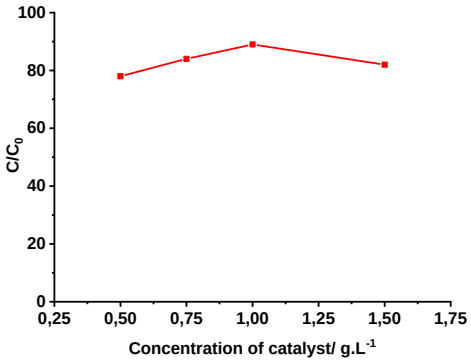

Figure 8. Effective of catalyst concentration to photodegradation of MB.

The role of pH in the photodegradation of organic pollutants, particularly in the removal of MB, is widely recognized as it significantly affects the production of hydroxyl radicals. To investigate this, the photodegradation of MB was carried out under visible light irradiation using $CuWO_4/g\text{-}C_3N_4$ as a catalyst over a range of pH values (3-9). The impact of pH on the photodegradation of MB is presented in Figure 9. It was observed that the photodegradation of MB was considerably enhanced at high pH and neutral pH. However, at low pH, the photodegradation of MB showed only moderate yield due to the substantial reduction of MB absorption on the surface of the catalyst, which impeded the removal of MB.

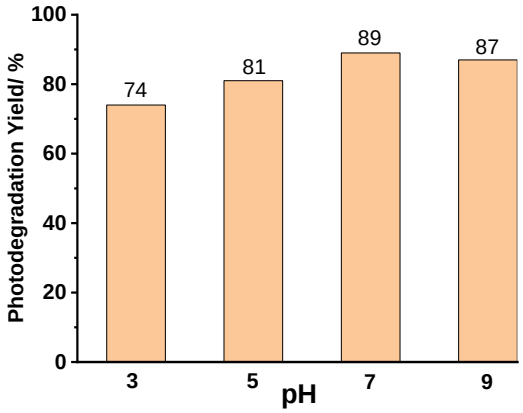

Figure 9. Effect of pH on photodegradation of MB.

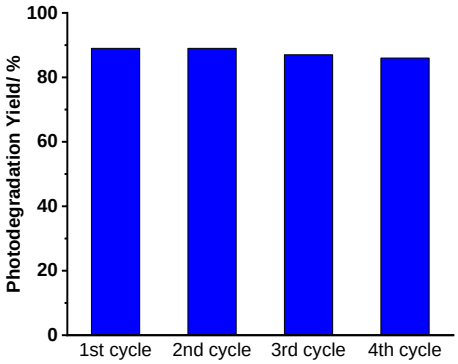

Figure 10. The recycling ability of $10\%CuWO_4/g\text{-}C_3N_4$ for photodegradation of MB.

Finally, the recycle ability of $10\%CuWO_4/g\text{-}C_3N_4$ for the photodegradation of DB 71 was investigated, and the results are presented in Figure 10. After an 80-minute irradiation time, the photocatalytic degradation efficiencies were over 85% after four cycles. These outcomes imply that the $10\%CuWO_4/g\text{-}C_3N_4$ is highly stable and can be used for long-term degradation processes.

4. Conclusion

Our objective is to investigate the viability of utilizing the novel $CuWO_4/g\text{-}C_3N_4$ nanocomposite for efficient degradation of MB through photodegradation under visible light irradiation. The results obtained from XRD, FT-IR, and SEM analyses confirmed the preservation of the $g\text{-}C_3N_4$ structure even after constructing $CuWO_4$, a finding further substantiated by SEM-EDS analysis. The UV-DRS results revealed that the $CuWO_4/g\text{-}C_3N_4$ materials exhibited higher activity than $g\text{-}C_3N_4$. Interestingly, the $10\%CuWO_4/g\text{-}C_3N_4$ composite significantly enhanced the photodegradation of MB within 80 minutes of visible light irradiation. The pH experiments demonstrated that $CuWO_4/g\text{-}C_3N_4$ displayed greater activity in neutral and alkaline pH conditions. Additionally, the $10\%CuWO_4/g\text{-}C_3N_4$ photocatalyst was stable and could be reused at least four times without declining its photocatalytic efficacy, making it highly desirable for practical applications.

Acknowledgements

The research was funded by the Vietnam Ministry of Science and Technology under grant number DTDL.CN-62/19.

References

[1] X. Yuan, L. Jiang, J. Liang, Y. Pan, J. Zhang, H. Wang, L. Leng, Z. Wu, R. Guan, G. Zeng, In-situ Synthesis of 3D Microsphere-like $In_2S_3/InVO_4$ Heterojunction with Efficient Photocatalytic Activity for Tetracycline Degradation under Visible Light Irradiation, Chemical Engineering Journal, Vol. 356, 2019, pp. 371-381, https://doi.org/10.1016/J.CEJ.2018.09.079.

[2] C. Arab, R. E. Kurdi, D. Patra, Effect of pH on the Removal of Anionic and Cationic Dyes using Zinc Curcumin Oxide Nanoparticles as Adsorbent, Mater Chem Phys, Vol. 277, 2022, pp. 125504, https://doi.org/10.1016/J.MATCHEMPHYS.2021.125504.

[3] S. Sharan, P. Khare, R. Shankar, A. Tyagi, A. Khare, Development of 3D Network of Zn-oxide Nanorods Assisted with PbO_2/Pb Electrode for Electrochemical Oxidation of Methylene Blue in Aqueous Phase, J. Taiwan Inst Chem Eng, Vol. 144, 2023, pp. 104739, https://doi.org/10.1016/J.JTICE.2023.104739.

[4] N. J. N. Nnaji, C. U. Sonde, O. L. Nwanji, G. C. Ezeh, A. U. Onuigbo, A. M. Ojukwu, P. C. Mbah, A. O. Adewumi, E. C. Unoka, J. O. Otedo, T. U. Onuegbu, Dacryodes Edulis Leaf Derived Biochar for Methylene Blue Biosorption, J. Environ Chem Eng, Vol. 11, 2023, pp. 109638, https://doi.org/10.1016/J.JECE.2023.109638.

[5] V. H. Huong, T. C. Nguyen, C. D. Sai, N. H. Pham, A. B. Ngac, T. B. Nguyen, H. V. Bui, V. P. Vu, B. T. Nguyen, L. V. Dang, T. T. H. Le, T. T. Nguyen, D. V. Do, Facile Synthesis of ZnO/Ag Nanostructure with Enhanced Photocatalytic Activity, ChemNanoMat, 2023, pp. e202300080, https://doi.org/10.1002/CNMA.202300080.

[6] A. Setiawan, L. R. Dianti, N. E. Mayangsari, D. R. Widiana, D. Dermawan, Removal of Methylene Blue using Heterogeneous Fenton Process with Fe Impregnated kepok Banana (Musa Acuminate L.) Peel Activated Carbon as Catalyst, Inorg Chem Commun, Vol. 152, 2023, pp. 110715, https://doi.org/10.1016/J.INOCHE.2023.110715.

[7] H. T. T. Duong, M. T. P. Duong, O. K. Nguyen, S. T. Le, L. V. Dang, B. T. Nguyen, D. V. Do, Photocatalytic Activity of Ti-SBA-15/C_3N_4 for Degradation of 2,4-Dichlorophenoxyacetic Acid in Water under Visible Light, J. Anal Methods Chem, 2022, https://doi.org/10.1155/2022/5531219.

[8] S. Faryad, U. Azhar, M. B. Tahir, W. Ali, M. Arif, M. Sagir, Spinach-derived Boron-doped g-C_3N_4/TiO_2 Composites for Efficient Photodegradation of Methylene Blue Dye, Chemosphere, Vol. 320, 2023, pp. 138002, https://doi.org/10.1016/J.CHEMOSPHERE.2023.138002.

[9] I. F. Waheed, M. A. Hamad, K. A. Jasim, A. J. Gesquiere, Degradation of Methylene Blue using a Novel Magnetic $CuNiFe_2O_4$/g-C_3N_4 Nanocomposite as Heterojunction Photocatalyst, Diam Relat Mater, Vol. 133, 2023, pp. 109716, https://doi.org/10.1016/J.DIAMOND.2023.109716.

[10] C. Yue, J. Jiang, M. Li, X. Wang, T. Li, Z. Zhao, S. Dong, Accelerating the Peroxymonosulfate Activation and Charge Transfer by Construction of Fermi Energy Level-matched $CoWO_4$/g-C_3N_4 Photocatalyst for Typical Antibiotics Degradation, Sep Purif Technol, Vol. 301, 2022, pp. 122020, https://doi.org/10.1016/J.SEPPUR.2022.122020.

[11] S. Sahoo, A. Behera, S. Mansingh, B. Tripathy, K. Parida, Facile Construction of $CoWO_4$ Modified g-C_3N_4 Nanocomposites with Enhanced Photocatalytic Activity under Visible Light Irradiation, Mater Today Proc, Vol. 35, 2021, pp. 193-197, https://doi.org/10.1016/J.MATPR.2020.04.246.

[12] V. Vinesh, M. Preeyanghaa, T. R. N. Kumar, M. Ashokkumar, C. L. Bianchi, B. Neppolian, Revealing the Stability of $CuWO_4$/g-C_3N_4 Nanocomposite for Photocatalytic Tetracycline Degradation from the Aqueous Environment and DFT Analysis, Environ Res, Vol. 207, 2022, pp. 112112, https://doi.org/10.1016/J.ENVRES.2021.112112.

[13] J. Anupriya, R. Rajakumaran, S. M. Chen, R. Karthik, J. V. Kumar, J. J. Shim, P. M. Shafi, J. W. Lee, Raspberry-like $CuWO_4$ Hollow Spheres Anchored on Sulfur-doped g-C_3N_4 Composite: An Efficient Electrocatalyst for Selective Electrochemical Detection of Antibiotic Drug Nitrofurazone, Chemosphere, Vol. 296, 2022, pp. 133997, https://doi.org/10.1016/J.CHEMOSPHERE.2022.133997.

[14] R. Gupta, B. Boruah, J. M. Modak, G. Madras, Kinetic Study of Z-scheme $C_3N_4/CuWO_4$

Photocatalyst Towards Solar Light Inactivation of Mixed Populated Bacteria, J. Photochem Photobiol A Chem, Vol. 372, 2019, pp. 108-121, https://doi.org/10.1016/J.JPHOTOCHEM.2018.08.035.

[15] S. Zhou, Y. Wang, G. Zhao, C. Li, L. Liu, F. Jiao, Enhanced Visible Light Photocatalytic Degradation of Rhodamine B by Z-scheme $CuWO_4$/g-C_3N_4 Heterojunction, Journal of Materials Science: Materials in Electronics, Vol. 32 2021, pp. 2731-2743, https://doi.org/10.1007/S10854-020-05003-0.

[16] N. T. T. Truc, T. D. Pham, D. V. Thuan, L. T. Son, D. T. Tran, M. V. Nguyen, V. N. Nguyen, N. M. Dang, H. T. Trang, Superior Activity of Cu-$NiWO_4$/g-C_3N_4 Z Direct System for Photocatalytic Decomposition of VOCs in Aerosol under Visible Light, J. Alloys Compd, Vol. 798, 2019, pp. 12-18, https://doi.org/10.1016/J.JALLCOM.2019.05.236.

[17] N. T. T. Truc, T. D. Pham, M. V. Nguyen, D. V. Thuan, D. Q. Trung, P. Thao, H. T. Trang, V. N. Nguyen, D. T. Tran, D. N. Minh, N. T. Hanh, H. M. Ngoc, Advanced $NiMoO_4$/g-C_3N_4 Z-scheme Heterojunction Photocatalyst for Efficient Conversion of CO_2 to Valuable Products, J. Alloys Compd, Vol. 842, 2020, pp. 155860, https://doi.org/10.1016/J.JALLCOM.2020.155860.

[18] N. T. Thanh Truc, N. T. Hanh, M. V. Nguyen, N. T. P. L. Chi, N. V. Noi, D. T. Tran, M. N. Ha, D. Q. Trung, T. D. Pham, Novel Direct Z-scheme $Cu_2V_2O_7$/g-C_3N_4 for Visible Light Photocatalytic Conversion of CO_2 into Valuable Fuels, Appl Surf Sci, Vol. 457, 2018, pp. 968-974, https://doi.org/10.1016/J.APSUSC.2018.07.034.

[19] A. Thomas, A. Fischer, F. Goettmann, M. Antonietti, J. O. Müller, R. Schlögl, J. M. Carlsson, Graphitic Carbon Nitride Materials: Variation of Structure and Morphology and Their use as Metal-free Catalysts, J. Mater Chem, Vol. 18, 2008, pp. 4893-4908, https://doi.org/10.1039/B800274F.